FETAL RADIATION DOSES IN COMPUTED TOMOGRAPHY EXAMINATIONS OF PREGNANT PATIENTS: A COMPARISON BETWEEN WHOLE-BODY AND INDIVIDUAL ORGAN DOSES AT THREE DIFFERENT GESTATIONAL AGES

By

NELIA SANCHEZ LONG

A THESIS PRESENTED TO THE GRADUATE SCHOOL
OF THE UNIVERSITY OF FLORIDA IN PARTIAL FULFILLMENT
OF THE REQUIREMENTS FOR THE DEGREE OF
MASTER OF SCIENCE

UNIVERSITY OF FLORIDA

2013

To my wonderful husband, for making me the happiest woman in the world
To my parents, for everything

ACKNOWLEDGMENTS

I thank Dr. Bolch for giving me this incredible opportunity and for his guidance throughout my graduate career. I thank Dr. John Aris, Dr. Manuel Arreola, and Dr. Lynn Rill for being part of my committee and for the help they have provided me. I thank Dr. Nash Moawad for sharing his knowledge and guidance in this project. I thank Dr. Roger Shifrin for his help collecting image sets. I thank my husband Dan, my family, and my colleagues and friends for their support and encouragement.

TABLE OF CONTENTS

page

LIST OF TABLES

LIST OF FIGURES

LIST OF ABBREVIATIONS

CT	Computed tomography
ICRP	International Commission on Radiological Protection
LOA	Left occipital anterior
MCNPX	Monte Carlo N-Particle eXtended
MRI	Magnetic resonance imaging
NURBS	Non-uniform rational B-spline
PACS	Picture Archiving and Communications System

Abstract of Thesis Presented to the Graduate School
of the University of Florida in Partial Fulfillment of the
Requirements for the Degree of Master of Science

FETAL RADIATION DOSES IN COMPUTED TOMOGRAPHY EXAMINATIONS OF PREGNANT PATIENTS: A COMPARISON BETWEEN WHOLE-BODY AND INDIVIDUAL ORGAN DOSES AT THREE DIFFERENT GESTATIONAL AGES

By

Nelia Sanchez Long

May 2013

Chair: Wesley Bolch
Major: Biomedical Engineering

The number of pregnant patients undergoing CT scans has been increasing by 25% every year; raising concerns among patients and doctors regarding the potential harmful effects of ionizing radiation on the developing fetus. An averaged radiation dose to the entire fetus may not always be sufficient to prospectively assess cancer risks for specific organs. Therefore, radiation doses received by each individual organ in the fetus during a CT exam are necessary to quantify these risks. This study used anatomic computational models of the pregnant female at 10, 25, and 38 weeks gestation to determine at what ranges of fetal size the average whole-body fetal dose would be sufficient to approximate the dose to specific fetal organs. Variations in radiation dose to a fetus with changes in maternal size as given by the maternal abdominal perimeter were also explored. Calculated CT doses for abdomen-pelvis exams for soft-tissue organs were at most 26% different than whole body averaged fetal doses. Homogeneous bone doses were at least 110% higher than whole-body doses in the 25- and 38-week models. Skeletal doses were as high as 25 mGy per 100 mAs per rotation.

Homogeneous bone doses in the 10-week model were less than 30% larger than the calculated whole-body dose. At greater gestational ages, the significant differences in results between the average whole-body dose and the skeletal dose during abdomen-pelvis CT exams should be considered when prospectively assessing leukemia risks. These risks may be underestimated if the whole-body dose is used instead of the skeletal dose.

CHAPTER 1
INTRODUCTION

A recent study by a research group at Brown University has shown an increase in the use of imaging examinations of pregnant females. In particular, the authors estimated that the use of computed tomography (CT) imaging on these patients will continue to increase by 25% each year.[1] This increase in usage has led to concerns regarding the effects and risks of in-utero radiation exposure to the fetus. These risks can be either deterministic or stochastic in nature. Deterministic effects, such as mental retardation, growth retardation, anatomic malformations, and death have a dose threshold of 100 mGy under which these effects would not be expected to occur.[2] On the other hand, there is no definitive dose threshold for stochastic effects (such as cancer), which may occur years after the initial irradiation event. Careful consideration needs to be given to the in-utero dose received by the fetus considering the higher radiosensitivity of rapidly dividing fetal tissues.

Although often avoidable, the use of CT diagnostic imaging on pregnant females is sometimes necessary, especially in cases where the pregnant patient is suspected of suffering from pulmonary embolism, acute appendicitis, or severe trauma. Acute pulmonary embolism is one of the leading causes of maternal mortality in the United States.[3] Recent studies have shown that multi-detector computed tomography (MDCT) pulmonary angiography is the overwhelmingly favored diagnostic procedure when screening for acute pulmonary embolism in pregnant patients. [4,5]

Additionally, acute abdominal pain occurs in 1 in 500 to 1 in 635 pregnancies while acute appendicitis has an incidence of 1 in 500 to 1 in 2000 pregnancies.[6] The occurrence of appendicitis has been shown to have the highest frequency in the third

trimester, with the second trimester being a close second.[7] Although there are alternative non-ionizing diagnostic exams available, such as ultrasound, MRI, and blood tests, the use of CT imaging is sometimes unavoidable. This need arises from the fact that an accurate diagnosis of acute appendicitis is often difficult to reach in pregnant patients (when only using ultrasound) given the displacement of the appendix caused by an enlarged uterus.[8] This difficulty becomes an important issue especially in the second and third trimesters of pregnancy. Accordingly, the rate of perforation surgery for these gestation stages is higher than that for the first trimester.[9,10] Therefore, although the use of ultrasound imaging is desirable as a non-ionizing alternative to CT; an accurate diagnosis is often limited because it depends on the position of the mother and anatomic movements which are of particular importance in the third trimester. Moreover, diagnostic tests for appendicitis are not reliable even when blood tests are performed in conjunction with ultrasound tests since they have shown to have a false negative rate of up to 50%.[11] False positive blood tests result in unnecessary appendectomies, a surgical procedure that increases mortality and morbidity.

Although diagnosis for acute appendicitis using MRI has been shown to provide comparable results and precision to CT imaging, equipment is often unavailable during emergency situations that are typical for acute appendicitis.[12,13] Therefore, even though MRI diagnostic tests are desired for its lack of harmful ionizing radiation to the fetus, surveys have shown that CT imaging is the preferred method of diagnosis for acute appendicitis and that it provides the most accurate diagnosis during pregnancy.[14,15]

There currently exist limits and recommendations with regard to in utero radiation dose limits. The International Commission on Radiological Protection (ICRP) has set

dose thresholds of 50-100 mGy for increased risks of deterministic effects such as malformations.[16] If estimates for the received fetal dose fall lower than these thresholds, the risks for deterministic effects is low enough that the dose should not be considered a reason to terminate the pregnancy. However, dose thresholds at which childhood cancers are not observed have not been established.[2] Furthermore, in order to be able to one day create risk estimates for specific types of childhood cancers, such as leukemia, individual fetal doses to soft-tissue organs as well as to fetal bone will be necessary. This study looks to explore the differences between the often-quoted averaged whole-body fetal dose and individual organ doses of the developing fetus. In order to do this however, computational models of the fetus and mother that are applicable to organ-level and bone-level radiation dosimetry are imperative.

Radiation doses to the fetus during a CT exam can be calculated using computational models of the radiation source (CT scanner) using Monte Carlo particle transportation methods as well as an anatomic computational model of the patient. For dose reconstruction purposes, the accuracy of the results achieved with this method greatly depends on the anatomical resemblance of the model.

There currently exist different types of computational fetal models used to assess fetal doses due to medical examinations. The different types of available fetal models include stylized (or mathematical), voxel (or tomographic), and hybrid (combination of polygon mesh or NURBS).

Early stylized models of the fetus are described by simple mathematical shapes and equations.[17] Although convenient and easy to use, these models do not provide a detailed differentiation of fetal skeletal and tissue structures needed for thorough

dosimetric studies. Advances in computing power have reduced the need to limit computational models to be described by only a few sets of simple surface equations.

An image-based specimen-specific fetal model created in 2004 had greater anatomical accuracy than the stylized models since it was based on in vivo CT images.[18] However, due to inherent limitations of these images this model did not take into account inhomogeneities in fetal bone tissue due to skeleton-associated cartilage.

There are also voxel models available that cover a range of gestational ages. These are patient-specific computational models created from a 24-patient retrospective study in which voxelized models of maternal and fetal anatomy were created. A very important correlation found by this study as a result of using these models in computational dosimetry was that fetal dose in CT is correlated to both maternal perimeter and fetal depth in the mother at the centroid of the fetus.[19]

In 2004 the first series of hybrid models of the pregnant mother and fetus was created based on three-dimensional reconstruction instead of voxels. The only organ-specific model in this series is limited to a model of the fetal brain taken from the stylized model.[20] Moreover, the fetal skeleton is approximately represented using the voxelized model of the image-based specimen-specific model discussed above. This series includes one model at the end of each trimester and can be used to estimate organ doses to the mother and the fetal skeleton, brain, and whole body.[21]

For the current study, the UF family of hybrid phantoms of the pregnant female was used to calculate fetal doses during CT examinations of the pregnant mother. This series of computational pregnant phantoms includes models at 8, 10, 15, 20, 25, 30, 35, and 38 weeks of gestation (post-conception). The fetuses in this series are 50% weight

percentiles at all gestational ages. The fetal library available however, also includes fetuses at 10% and 90% weight percentile at 20 weeks and older. The UF series is the most thorough and detailed set of fetal models presently available. These models account for variations in skeletal size and proportion, variations in relative levels of bone ossification, and variations with age in individual organ masses and total fetal masses.[22] Therefore, when calculating doses to assess stochastic risks the UF family of hybrid models is the most appropriate since it allows for calculation of organ-level and bone-level radiation dosimetry.

CHAPTER 2
MATERIALS AND METHODS

Collection and Analysis of Image Sets of Pregnant Patients

A series of retrospectively-collected CT and MR images of pregnant patients covering a range of gestational ages and maternal sizes was collected and reviewed for this study. Data sources included both the PACS image archives of the University of Florida Department of Radiology and those published electronically from a UCLA study in 2008.[19] A total of 79 CT image sets in which the fetus was fully visible were collected for use in this study. From these retrospectively collected images, a candidate image set for each gestational age was chosen based on agreement of the segmented fetal volume and the target reference fetal volume of the UF family of fetal models.[22] All pregnant female images were reviewed by Roger Shifrin, MD, a practicing radiologist, and by Nash Moawad, MD, a physician with a specialty in obstetrics and gynecology, to ensure normality of the maternal anatomy. Each image set was segmented to record and obtain information regarding changes and displacements of organs and anatomy in the pregnant female. These image sets were used by PhD candidate Matthew Maynard to create an array of pregnant computational models that uniquely accommodate each of the UF series of reference fetal hybrid phantoms. The UF reference adult female hybrid phantom was used as a starting model for construction of the pregnant model.[23] Using the information obtained from image segmentation, he was then able to accommodate all changes in maternal anatomy for all 8 gestational ages. Under Dr. Moawad's guidance, Mr. Maynard placed the fetus in a left-occipital anterior (LOA) position due to it being one of the most common positions in pregnancy.

Fetal Model

Since differentiation of fetal organs is essential when estimating cancer risks as well as for retrospective radiation epidemiology studies, a decision was made to utilize the UF series of reference pregnant models for this study. Specifically, the fetal skeleton is the most critical organ of interest when assessing childhood leukemia risks. The UF series of pregnant/fetal models provides a much finer variation of fetal ages that span the extent of a typical pregnancy, offers detailed anatomical models of all major organs and has a skeleton that includes both ossified homogeneous bone and unossified cartilage for each major bone site It also considers different statistical percentiles for most fetal ages regarding fetal skeleton size, individual organ masses, and total fetal mass. Figure 1-2 shows the 50^{th} percentile fetal model used in this study at each of the three gestational ages.

Reshaping the UF Reference Pregnant Computational Model

Although the UF family of reference pregnant computational models includes a total of 8 gestational ages at 8, 10, 15, 20, 25, 30, 35, and 38 weeks post-conception (PC), this study only explored the models at 10, 25, and 38 weeks, which correspond to the end of each trimester of gestation. The fetal models in each of the three ages are the 50^{th} percentile models previously constructed by Mr. Maynard. Under the guidance of Dr. Nash Moawad, the maternal adipose layer of each of the three reference pregnant models was reshaped and adjusted to fit 9 models at each gestational age. The outer-body contouring of each of the reference pregnant models at these three gestational ages was adjusted to include a wider range of maternal perimeters at fetal centroid by systematically increasing and decreasing the subcutaneous fat layer. The

adipose tissue layer was increased proportionally around the abdomen, buttocks, and back of the model of the mother. For the largest (overweight) models at each gestational age the volumes of the arms, legs, and breasts were increased by 30% from reference values. This resulted in a total of 9 different maternal sizes per each of the 3 gestational ages explored in this study. The maternal circumferences at fetal centroid ranged from 85 cm to 125 cm, 95 cm to 125 cm, and 100 cm to 140 cm for the 10-, 25-, and 38-week fetal models, respectively. The median at each gestational age was then chosen as the reference pregnant model with the approval of Dr. Moawad. Figure 1-3 shows the reference model at each of the three gestational ages.

CT Simulated Exams

Dual-Lattice MCNPX Inputs

In order to achieve acceptable uncertainties and reliable dose results from MCNPX, the voxel sizes in the computational model of the fetal organs need to be small enough with respect to the organ size itself. However, it is time-prohibitive to voxelize the entire model, which includes both maternal and fetal organs, at these minute voxel sizes. Therefore, it became necessary in this study to implement a dual-lattice MCNPX input in which the voxel sizes for fetal organs were up to 3220 times smaller than those of the mother. Figure 1-2 shows an example of the dual-lattice universe in MCNPX for the 25-week model.

CT Source Model and Scan Parameters

In collaboration with Daniel Long, a PhD candidate in medical physics, organ and whole-body doses were calculated using MCNPX Version 2.7. The source subroutine used was a model of the Toshiba Aquilion ONE CT scanner operating in 64-slice mode. It was previously developed as part of Mr. Long's doctoral research and has been

experimentally validated against computed tomography dose index (CTDI) phantom measurements. The subroutine allows for the user to select scan parameters such as beam energy, filtration, pitch, beam collimation, and scan length.

Provided in Table 1-1 are the parameters used for the abdomen-pelvis and chest CT exams. These values were chosen based on standardized protocols historically used at Shands Hospital at the University of Florida.

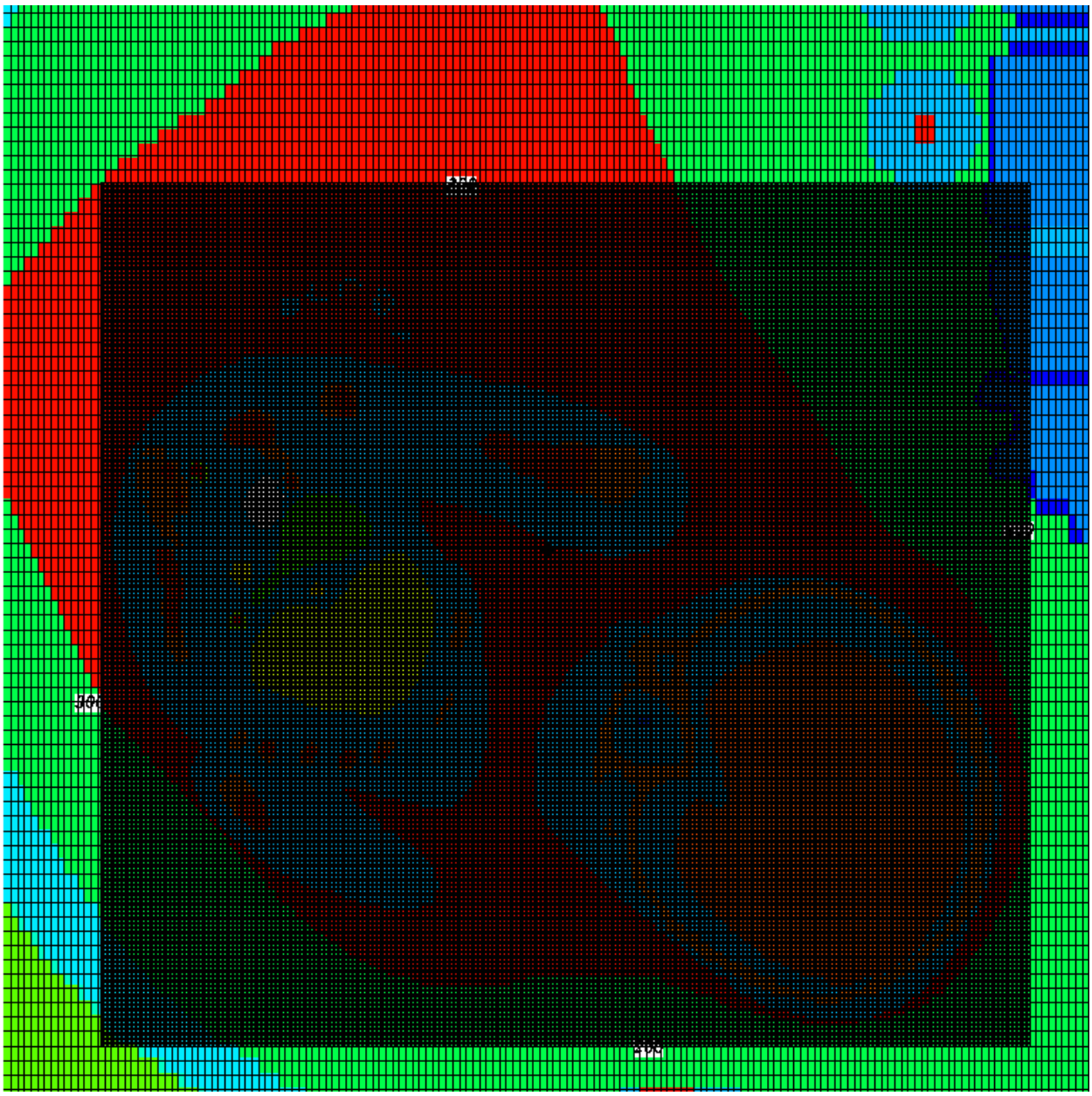

Figure 1-1. Dual-lattice in MCNPX for the 25-week fetus

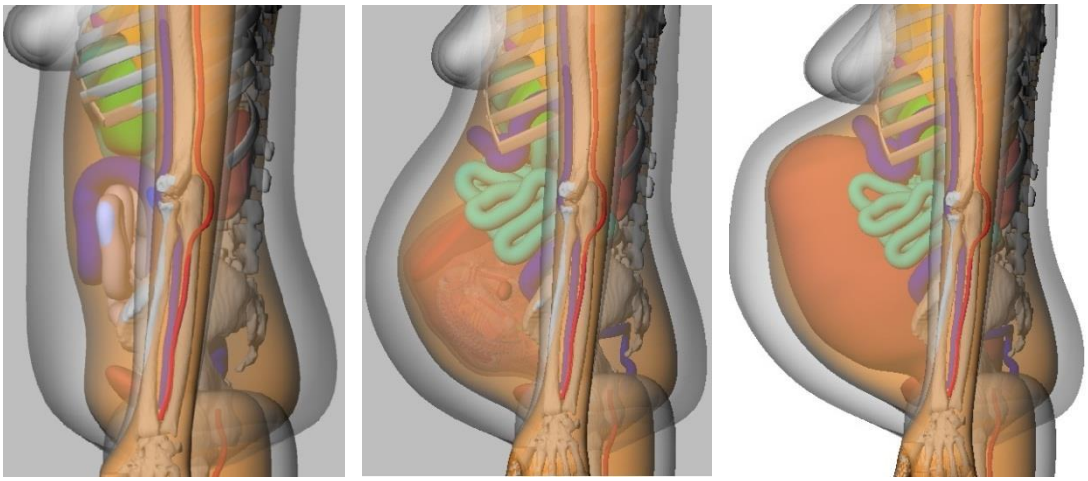

Figure 1-2. Reference models at A) 10 weeks, (B) 25 weeks, (C) 38 weeks

Table 1-1. CT scan parameters

Parameter	AP	Chest
Scan start	Dome of diaphragm	Thoracic inlet
Scan end	Lesser trochanter	Top of Kidneys
Energy	120 kVp	120 kVp
Filtration	Large	Large
Detector configuration	64 x 0.5mm	64 x 0.5mm
Pitch	0.828	0.828
Tube current-time product	100 mAs	100 mAs

CHAPTER 3
RESULTS AND DISCUSSION

Abdomen-Pelvis CT Exam

Figures 3-1 to 3-3 show the organ dose results from simulated runs, including MCNPX reported uncertainties, for the abdomen-pelvis CT exam in the 38-week, 25-week, and 10-week model, respectively, at all 9 available maternal sizes. The whole-body dose was calculated by adding all organ tallies and dividing them by the summation of all tallied organ masses. A tube current-time product of 100 mAs per rotation was assumed for comparison purposes. For the abdomen-pelvis simulated exam, the entire fetus was in the field of view at all three ages. The data for each fetal organ dose was fitted using a linear-regression method of least squares at all three gestational ages. The resulting coefficient of determination (r-squared) value for both the 25- and 38-week models was at least 0.99. For the 10-week model, the r^2 value had an average, standard deviation, and minimum of 0.91, 0.05, and 0.8, respectively. The relatively larger dose uncertainties in the 10-week model were a result of computational limitations in terms of the feasible number of particle histories in MCNPX.

It is important to note that these reported doses should not be misinterpreted as absolute fetal doses received in an actual CT examination. Namely, it does not necessarily follow that for a given fetal size the individual organ doses to the fetus will decrease with maternal size. On the contrary, organ doses at higher maternal circumferences will likely increase due to the fact that larger patients require a higher mAs value to acquire an acceptable image quality. For comparison purposes however, all doses in this study were normalized to 100 mAs/rotation. In the future, fetal doses as

a function of maternal size will be explored using the computational models developed in this study as well as by applying size-dependent beam output parameters.

The marked difference in results between homogenous bone and the rest of the individual organ doses is mainly a result of differences in the mass energy-absorption coefficient of the bone when compared to other soft-tissue organs. This can be easily observed in Figure 3-4 where organ doses have been normalized to this value for the 38-week dose results. The relative difference between soft-tissue organs and homogenous bone then becomes much less pronounced and any differences remaining pertain to shielding effects and varying distances from the beam source.

Displayed in Figure 3-5 is a comparison of the simulated fetal organ doses as well as for the calculated whole-body dose between the three gestational ages for the reference model at each age. It is important to note that although the energy deposition per particle in MCNPX for the 38-week organs was higher than that for the 25-week model, the dose per 100 mAs/rotation was ultimately lower due to the mass increase per organ between the two ages being greater than the increase in energy deposition. This effect is shown in Figure 3-6 where it is easily observed that the 38-week to 25-week ratio of organ masses is greater than the ratio of energy deposition per particle. Interestingly, this ratio is very close to 1 for the skeleton and therefore the resulting doses are very similar for these two ages. It should also be noted once again that these doses should only be used for comparison purposes; a larger patient will require a higher beam output (mAs) and therefore, the dose delivered to the fetus will likely be higher in the 38-week model in a clinical scenario.

After analyzing this data, it became apparent that as gestational age increases, absorbed doses seem to follow a sort of distribution in which a maximum dose is reached in the middle gestational age. This is due to the fact that there are three major factors affecting doses delivered to the fetal organs during CT examinations: (1) the size of the mother, (2) the relative location (superficial or deep) of the fetus within the mother, and (3) the radiation interaction characteristics of each organ. While a larger maternal size will tend to decrease fetal doses per 100 mAs, a more superficially-located fetus will receive a larger dose than a fetus located deeper within the mother. Therefore, despite the fact that in the 10-week model the mother was smaller in size, the fetus received a lower dose due to its deep location. The 25- and 38-week fetuses both had about the same relative superficial location within their respective maternal models, but since the 25-week mother was smaller than the 38-week mother it resulted in larger doses delivered to the 25-week fetus.

Provided in Figure 3-7 are these same individual fetal organ doses normalized to whole-body dose per gestational age for each reference-size model. As can be observed, individual soft-tissue organ doses at all three gestational ages stayed relatively close to the calculated whole-body dose. Average percent differences between individual soft-tissue organ doses and whole-body doses can be found in Table 3-1.

On the other hand, easily shown in Figure 3-7 is the significant difference that occurs at the two oldest ages between homogeneous bone doses and whole-body dose. Percent differences between homogeneous bone and whole-body doses can be found in Table 3-1. These large differences in the oldest two models are due to the fact

that the mass-energy absorption coefficient is in both cases is an order of magnitude higher than that of the other organs. Therefore, radiation interactions in the bone will result in higher energy deposition. The 10-week model does not show this trend due to the fact that at this young age the skeleton has barely ossified and the mass energy-absorption coefficient is in the same order of magnitude as that for the soft-tissue organs.

Since the difference between soft-tissue doses and skeletal doses for the 25-week model were less than that for the 38-week model, the whole-body dose was therefore closer to individual organ doses in the 25-week (Table 3-1). This can be attributed to a more defined dose gradient across the fetus in the older (and therefore larger) gestational ages. It can be concluded therefore, that for larger fetuses, the dose-gradient will have a greater effect on individual organ doses and the difference across organs will be more apparent.

The substantial differences between whole-body dose and homogeneous bone in the fetus could have significant implications when used for prospective assessments of radiogenic leukemia risks as well as radiogenic bone cancer risks. Important to note is the fact that although fetal bone in the utilized phantoms was modeled as a homogeneous tissue consisting of cortical bone and spongiosa, a recent study has found that in newborns, the percentage of cortical bone is 40% while trabecular bone is 60%.[24] Consequently, most of the dose delivered to the skeleton will in fact be deposited in trabecular bone, where radiosensitive bone marrow cavities with hematopoietic cells are found. The homogeneous bone doses computed in this study were as high as 23 mGy per 100 mAs per rotation. This number could reach 69 mGy or

more if clinically implemented tube current-time product values of 300 mAs were applied. In our retrospectively-collected data, constant tube-current values for AP exams had an average value of 278 mAs and a standard deviation of 103 mAs.

Chest CT Exam

Figures 3-8 to 3-10 show the organ dose results from simulated runs, including MCNPX reported uncertainties, for the chest CT exam in the 10-week, 25-week, and 38-week model, respectively, at all 9 available maternal sizes. A tube current-time product of 100 mAs per rotation was assumed for comparison purposes. For the simulated chest exam the entire fetus was out of the field of view at all three ages. Therefore, all dose received was a result of scatter radiation off of the maternal model. The data for each fetal organ dose was fitted using a linear-regression method of least squares at all three gestational ages. However, the resulting coefficient of determination (r-squared) value for all three gestational ages was too low to be acceptable. This is mainly due to the fact that MCNPX uncertainties for this model ranged from 3% to 70%. The relatively larger dose uncertainties in the 10-week model were a result of computational limitations in terms of the feasible number of particle histories in MCNPX. Statistics in the 10-week model are inherently worse, and therefore require more particle histories because the target volumes are exceptionally small and fewer particles are reaching it. It can be observed in Figures 3-8 to 3-10 that absorbed doses to a given organ stayed relatively constant across maternal sizes when assuming a constant tube-current time product of 100 mAs. This is merely due to the fact that maternal size around the fetus does not play an important role when the scatter sources are tissues in the maternal chest area. In this direction, the amount of tissue between the scatter source and the fetus remains constant in the pregnant model.

As expected, the calculated fetal doses for this exam were much lower than those for the abdomen-pelvis exam using the same pregnant model. Individual organ doses were on average 63, 46, and 27 times higher in the abdomen-pelvis exam than in the chest exam for the 10-week, 25-week, and 38-week model, respectively. All computed doses were less than 1.5 mGy. This is primarily due to the fact that during a chest CT exam the fetus is not directly in the radiation beam and therefore the dose delivered to the fetus is a result of scatter radiation off of the maternal tissues that are in the direct path of the radiation beam. The inverse-square law explains why doses increase as a function of age for a chest exam since the fetus is located lower in the pelvic region at the younger gestational ages and gets much closer to the scatter source as it grows and starts to occupy the upper abdominal region of the mother. This can be observed in Figure 1-2.

Fetal homogeneous bone was once again higher than the rest of the soft-tissue organs as well as the calculated whole-body due to differences in the mass energy-absorption coefficient. Dose to organs in the chest exam increased with gestational age, excluding the brain. These results are consistent with those obtained by a recent study which observed a similar trend between soft-tissue organ doses for three similar fetal sizes.[25] This study concluded that skeletal organ doses decreased with increasing age, however, the doses provided by that study were very similar for the two gestational ages and no uncertainties were reported.

Displayed in Figure 3-11 is a comparison of the simulated fetal organ doses as well as for the calculated whole-body dose between the three gestational ages for the reference model at each age. As can be observed, organs closest to the chest obtained

higher doses than those farther away. Provided in Figure 3-12 are these same individual fetal organ doses normalized to whole-body dose per gestational age for each reference-size model.

Overall, although homogeneous bone doses were more than twice as large as calculated whole-body doses, the maximum dose received was around 1mGy. These absorbed doses are at least an order of magnitude smaller than homogenous bone doses for the abdomen-pelvis exam. Therefore, chest skeletal doses are of less relative concern as compared to the abdomen-pelvis doses when assessing cancer risks.

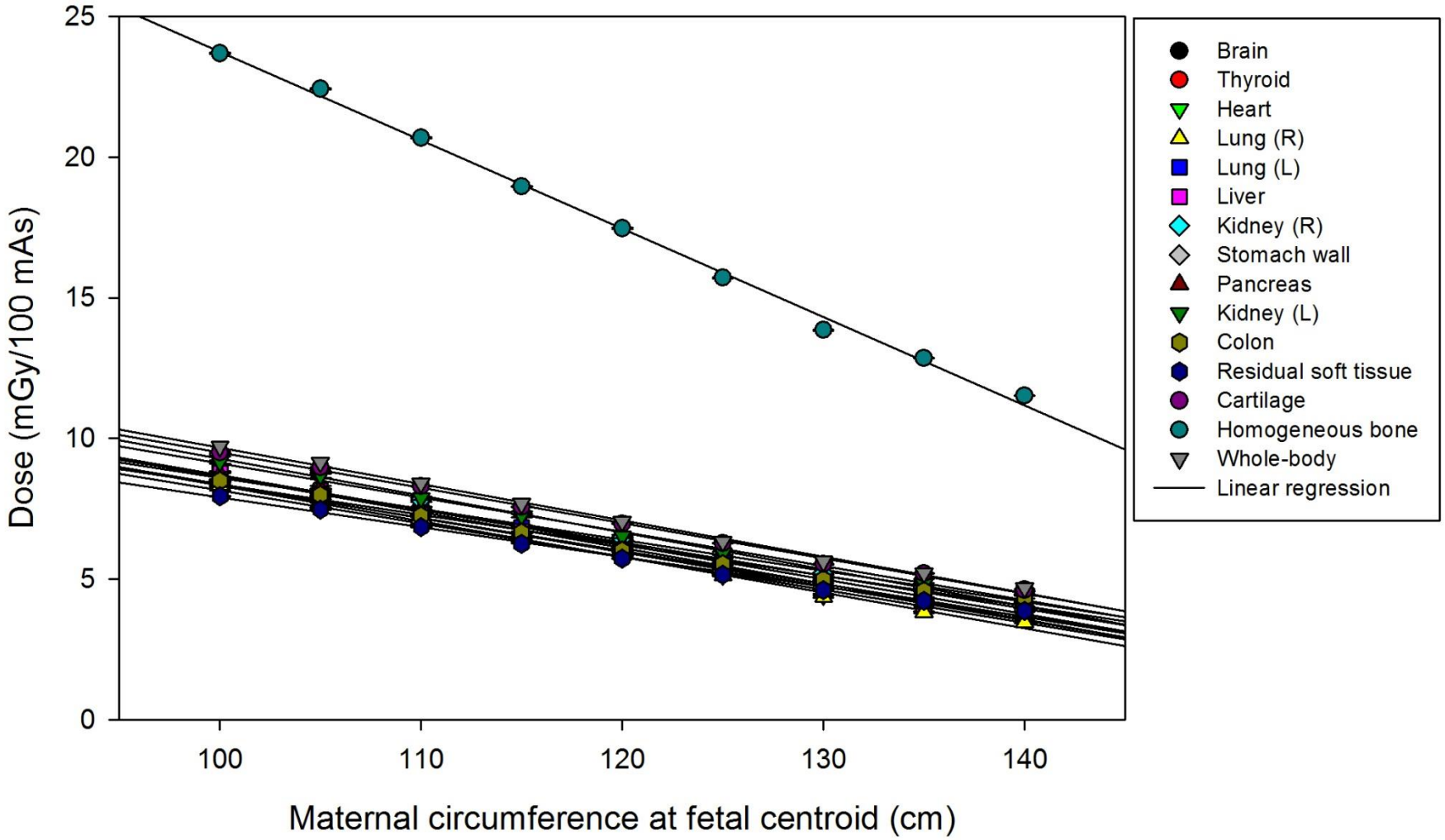

Figure 3-1. Abdomen-pelvis exam organ and whole-body doses as a function of maternal size at 38 weeks of gestation

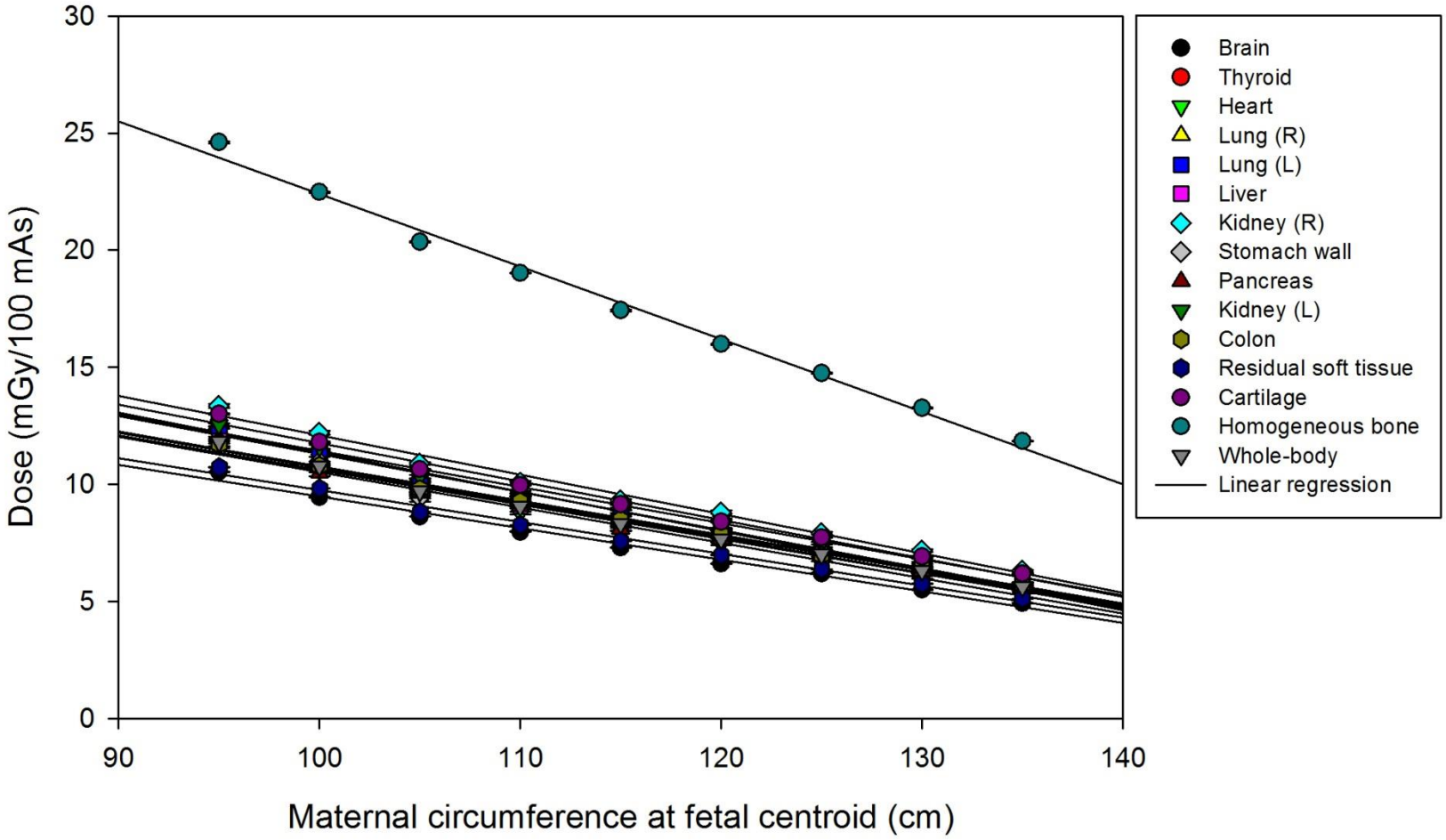

Figure 3-2. Abdomen-pelvis exam organ and whole-body doses as a function of maternal size at 25 weeks of gestation

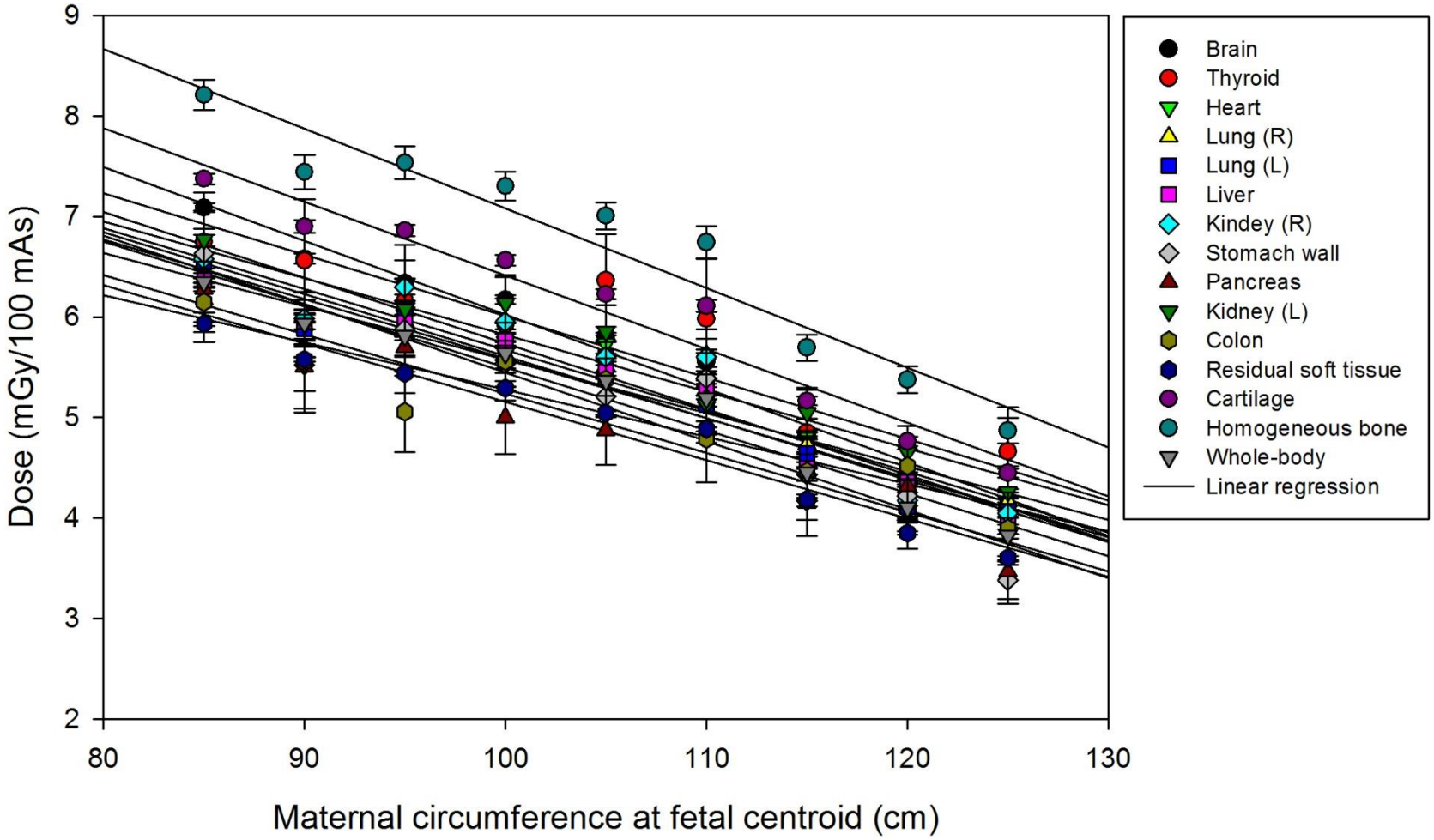

Figure 3-3. Abdomen-pelvis exam organ and whole-body doses as a function of maternal size at 10 weeks of gestation

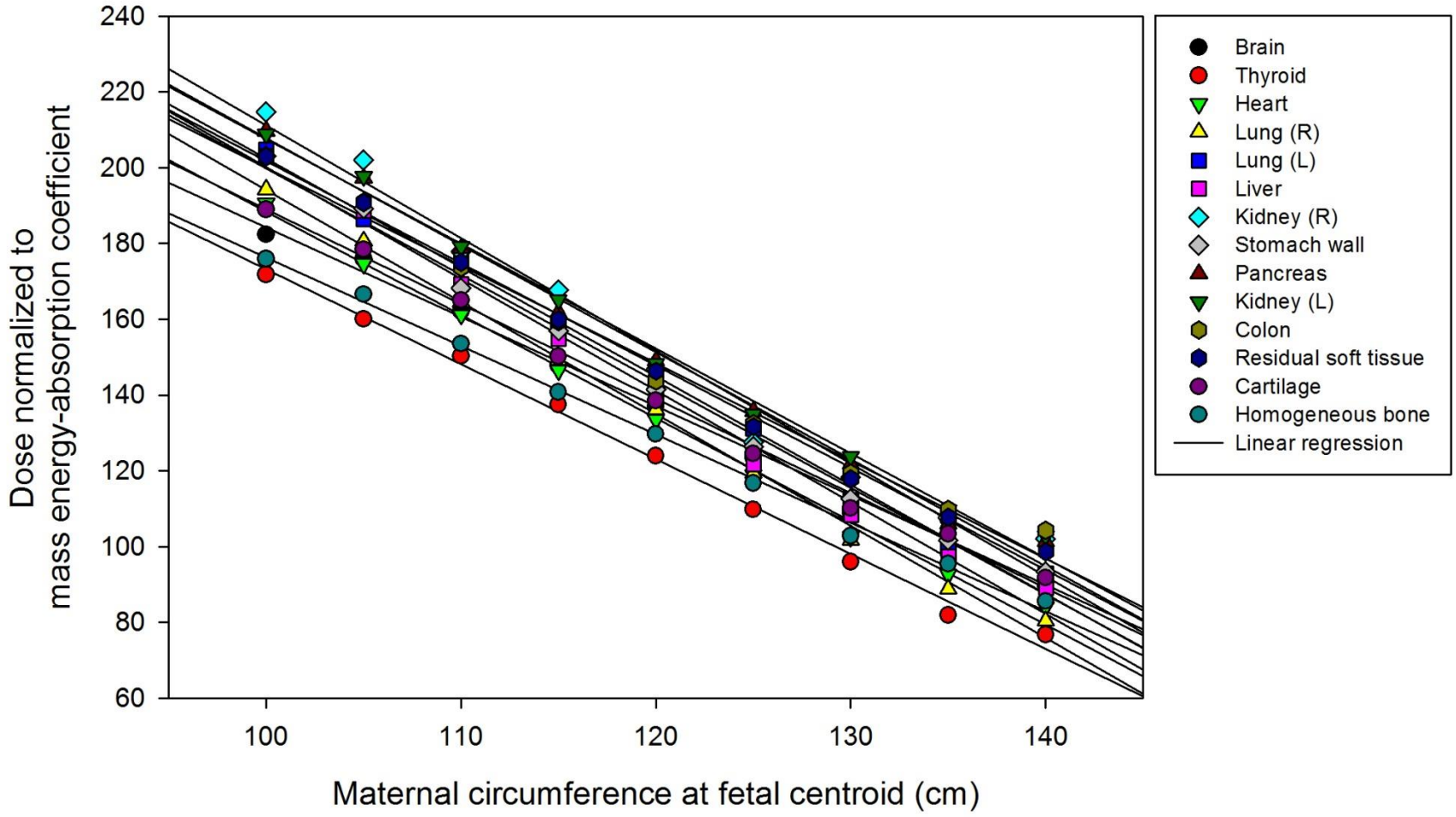

Figure 3-4. Abdomen-pelvis exam organ doses normalized to the mass energy absorption coefficient for the 38-week model

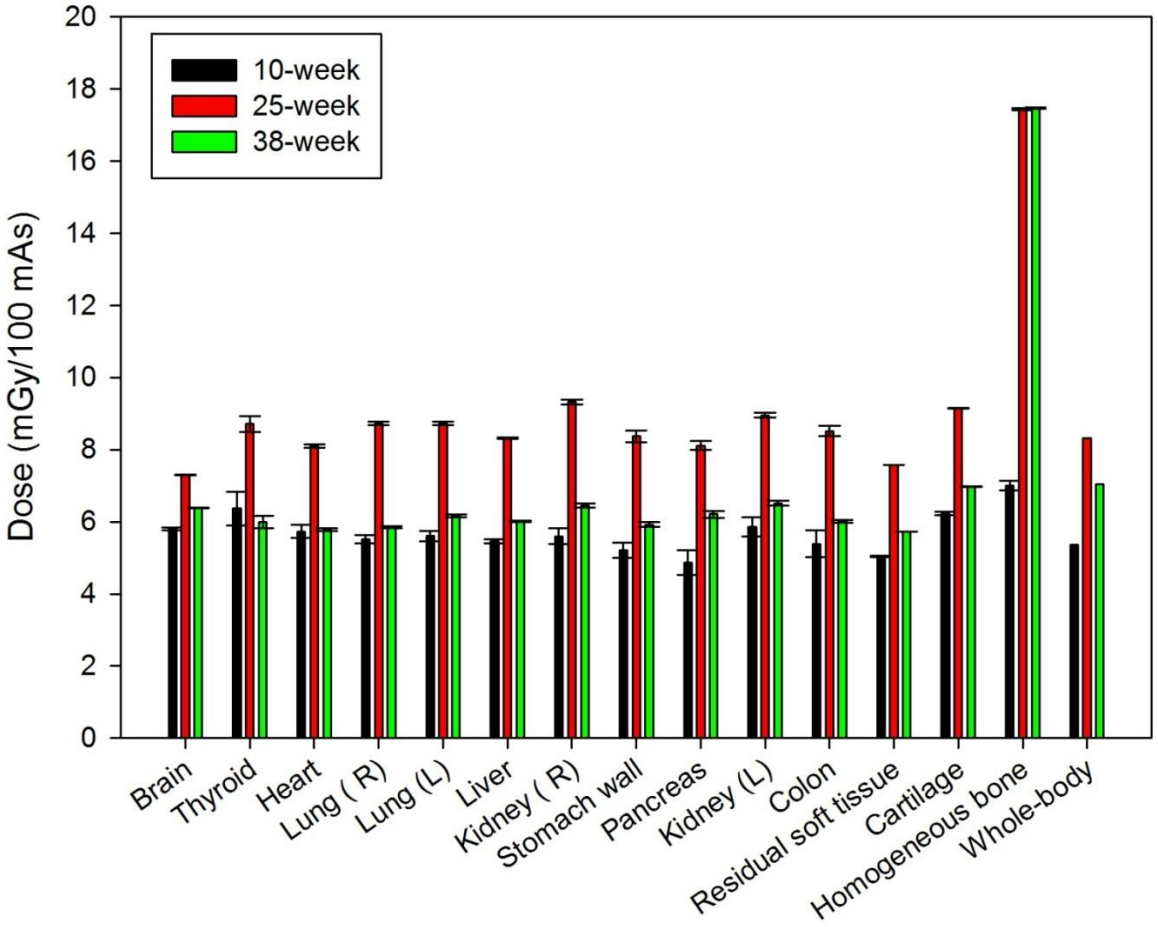

Figure 3-5. Abdomen-pelvis exam individual organ and whole-body dose at all three ages for the reference-size model

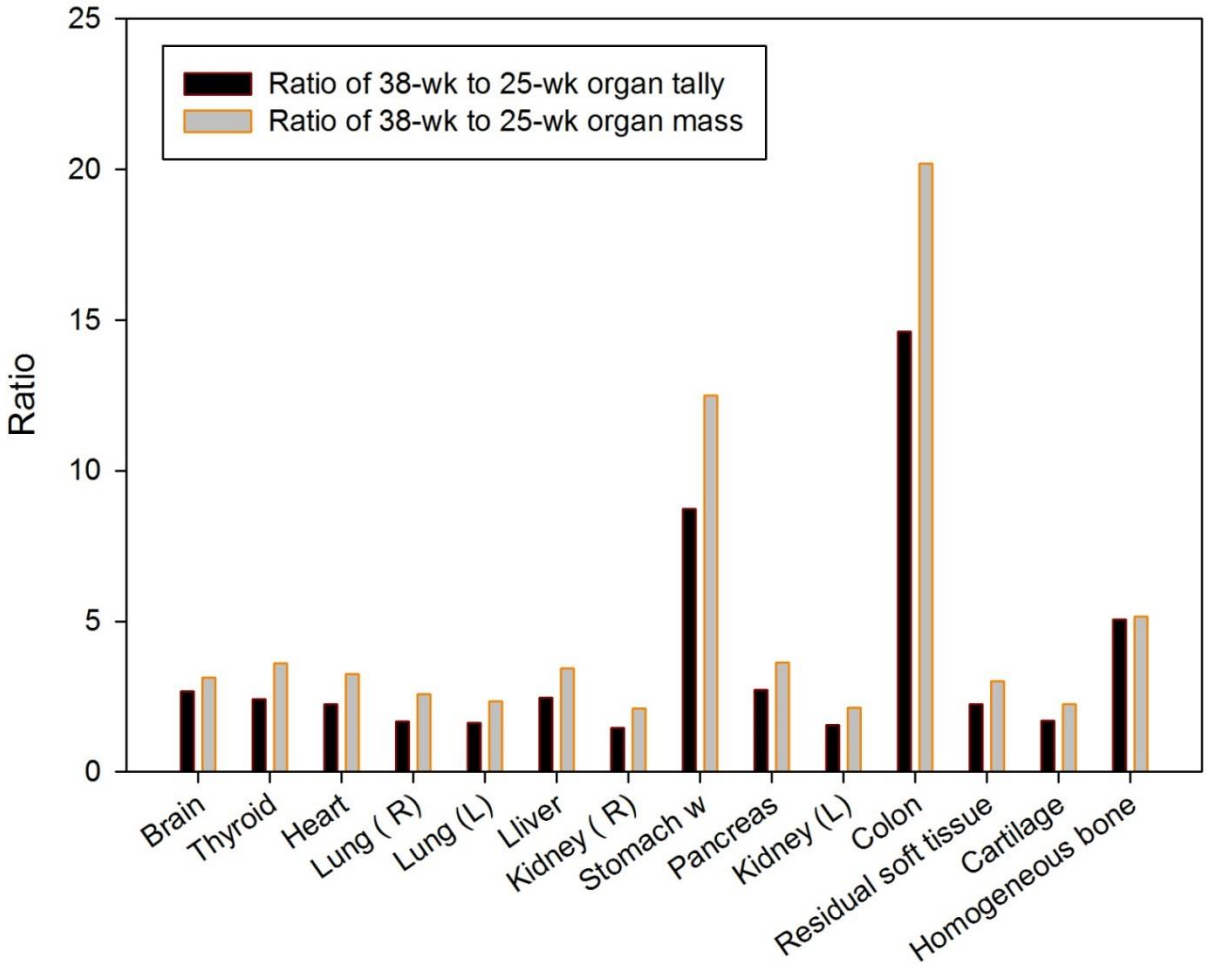

Figure 3-6. Abdomen-pelvis exam average ratios of organ tallies and organ masses between the 38- and 25-week model

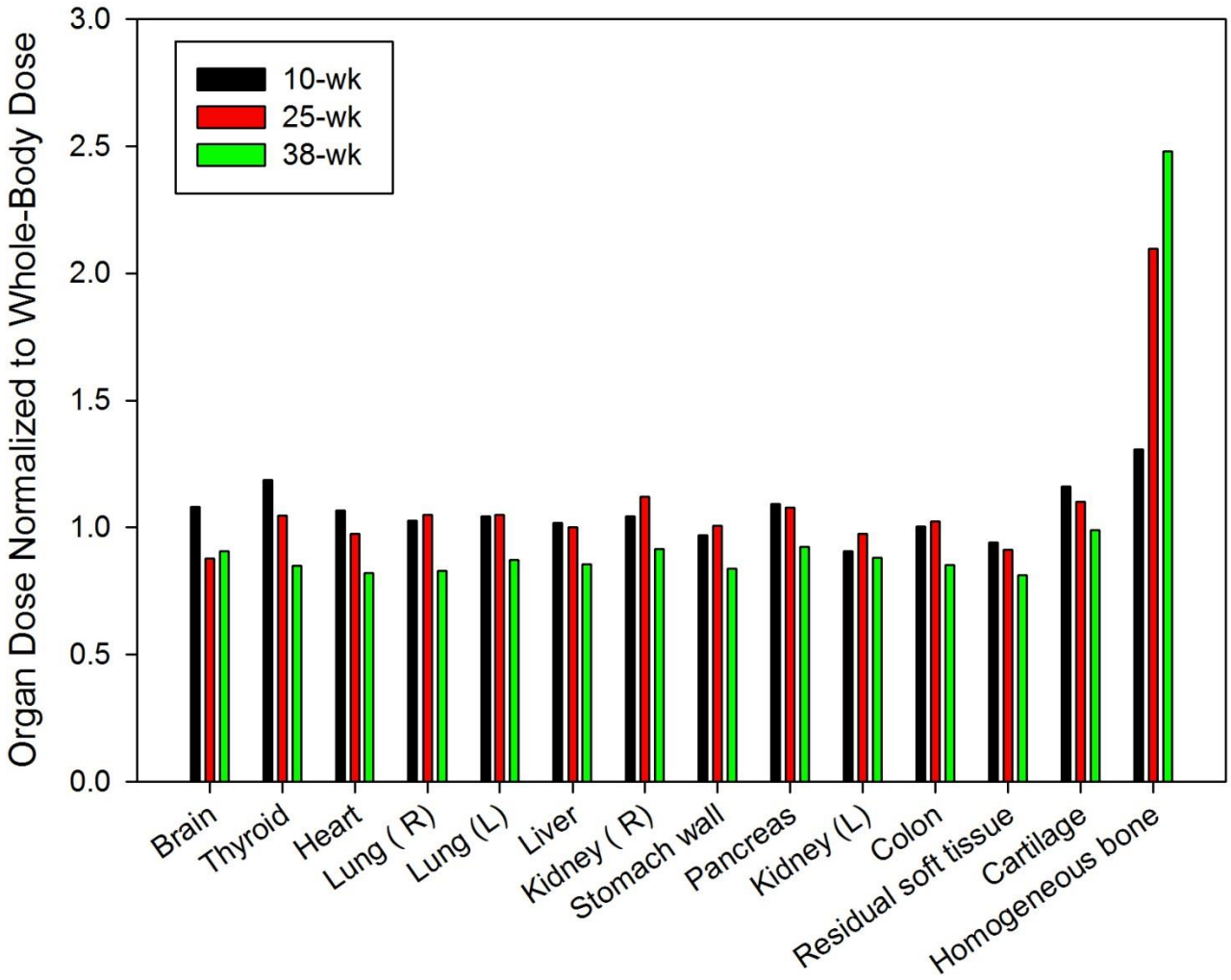

Figure 3-7. Abdomen-pelvis exam organ doses normalized to whole-body dose at all three gestational ages for the reference model

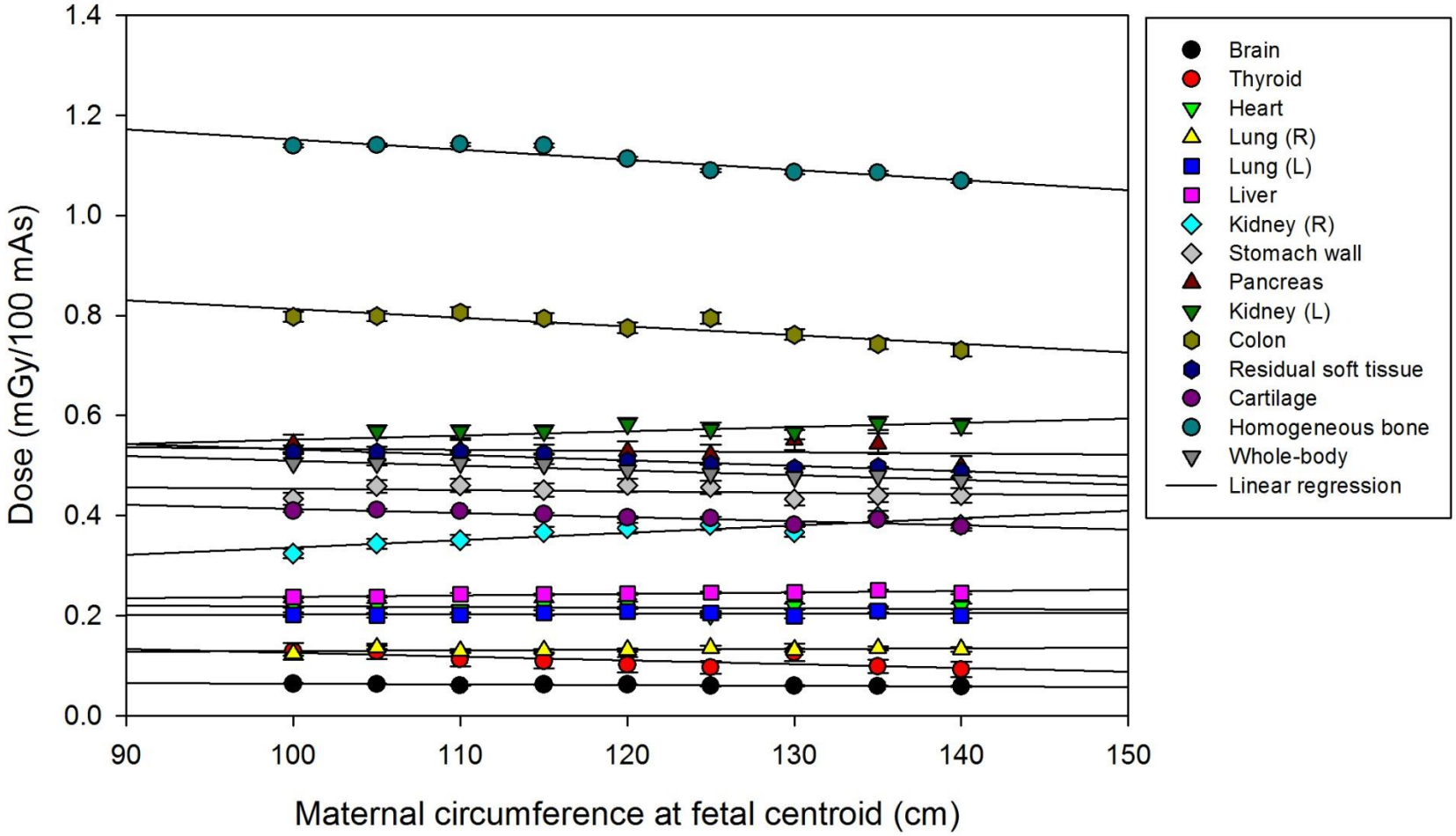

Figure 3-8. Chest exam organ and whole-body doses as a function of maternal size at 38 weeks of gestation

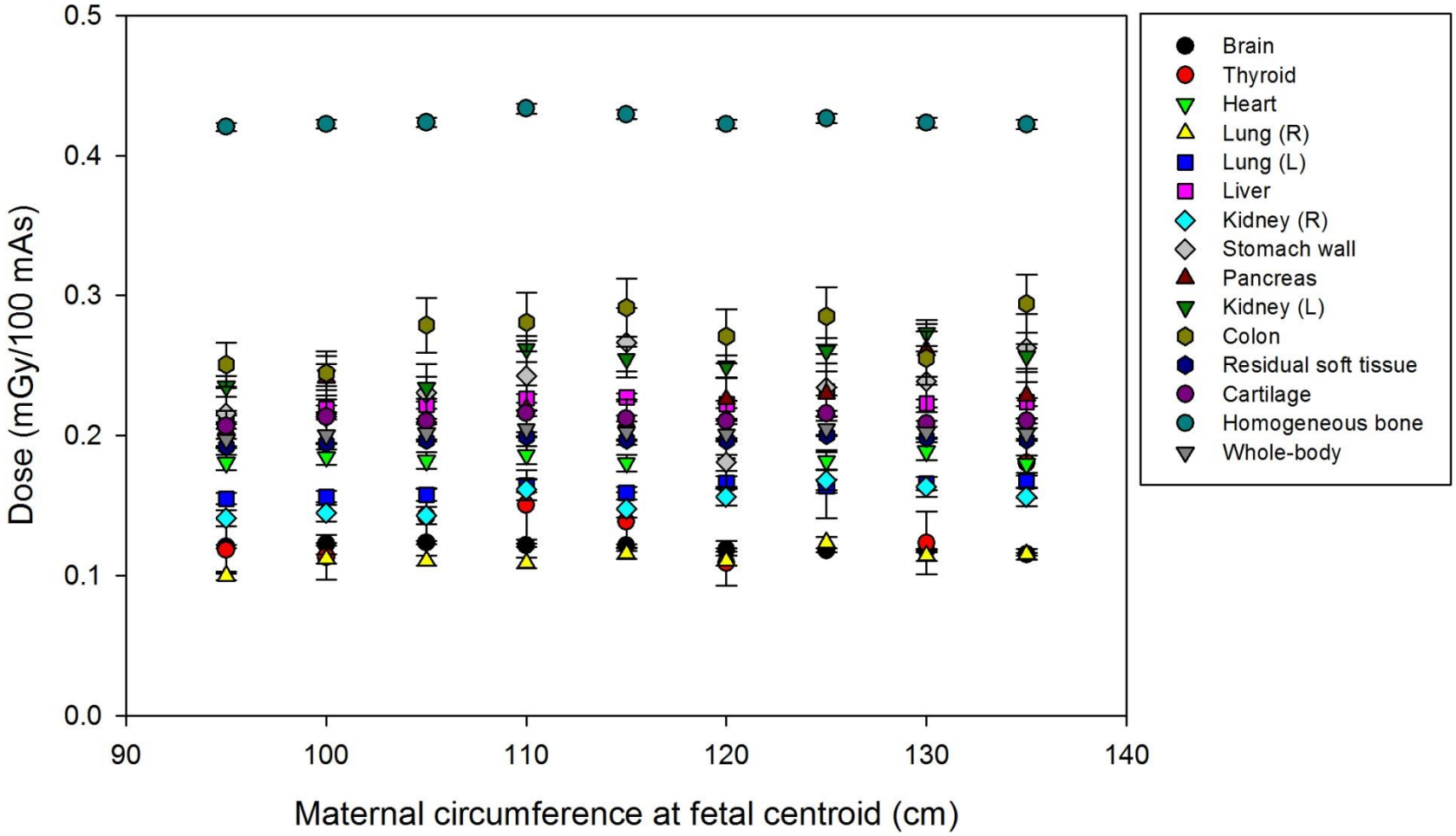

Figure 3-9. Chest exam organ and whole-body doses as a function of maternal size at 25 weeks of gestation

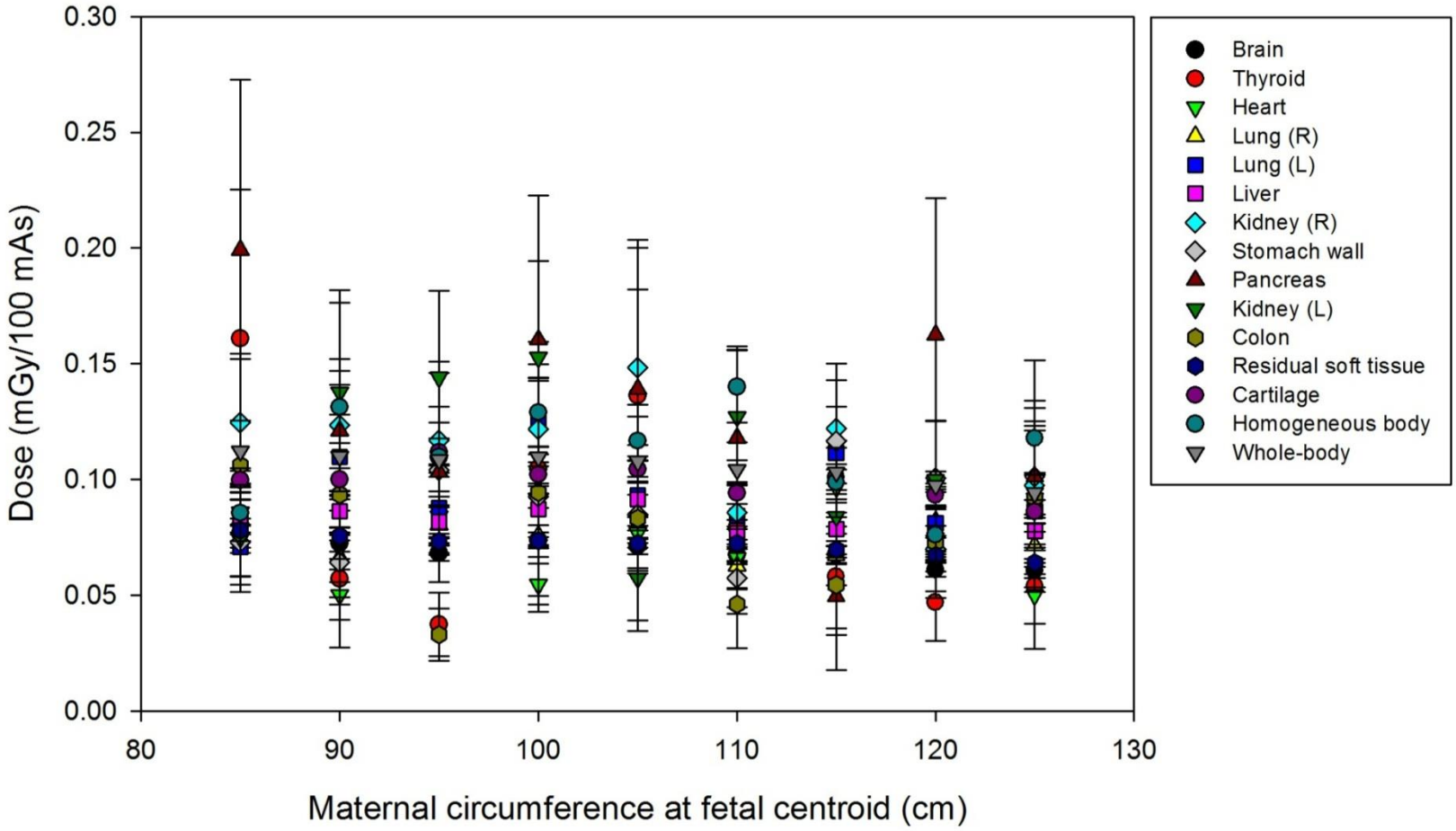

Figure 3-10. Chest exam organ and whole-body doses as a function of maternal size at 10 weeks of gestation

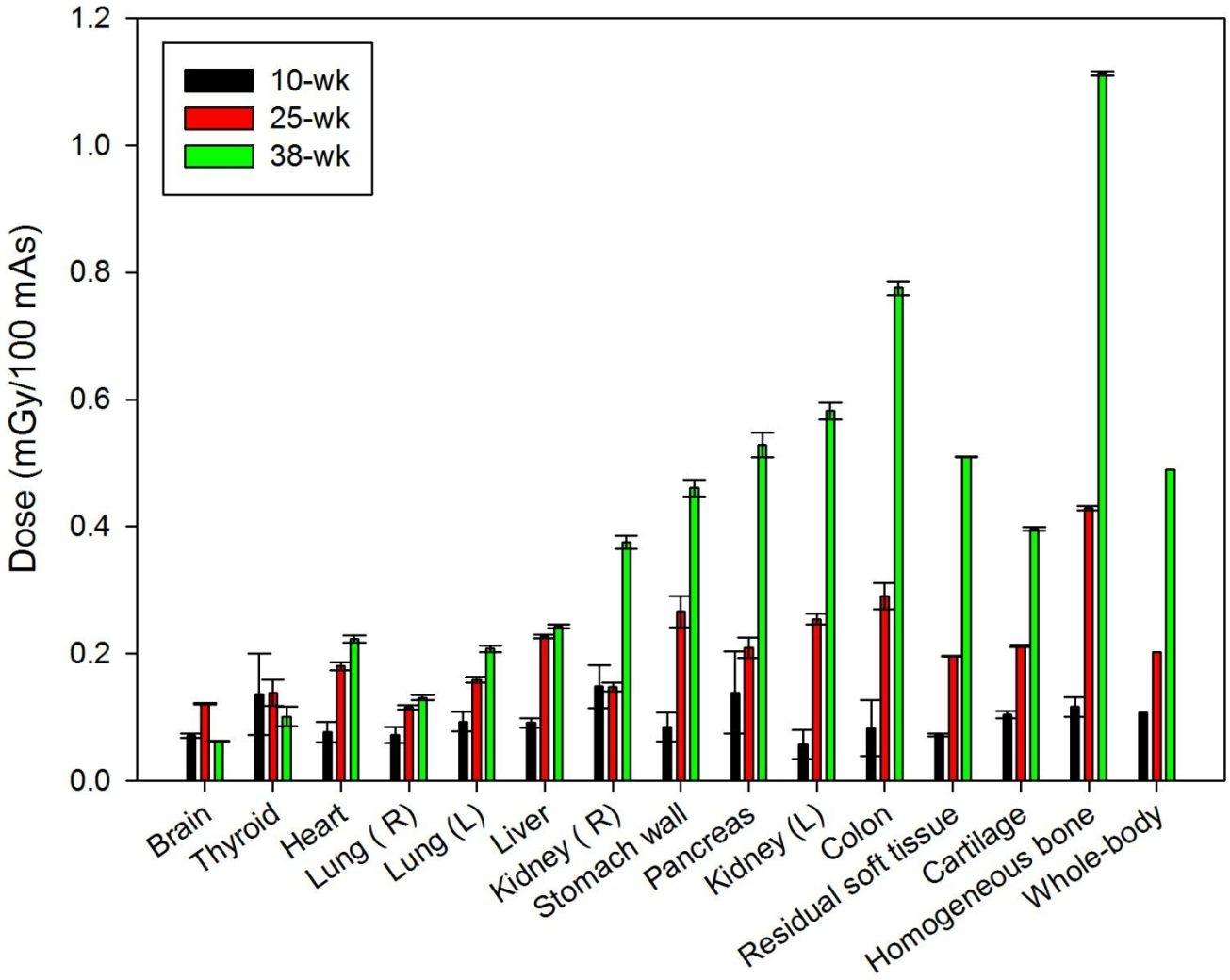

Figure 3-11. Chest exam organ and whole-body doses at all three ages for the reference-size model

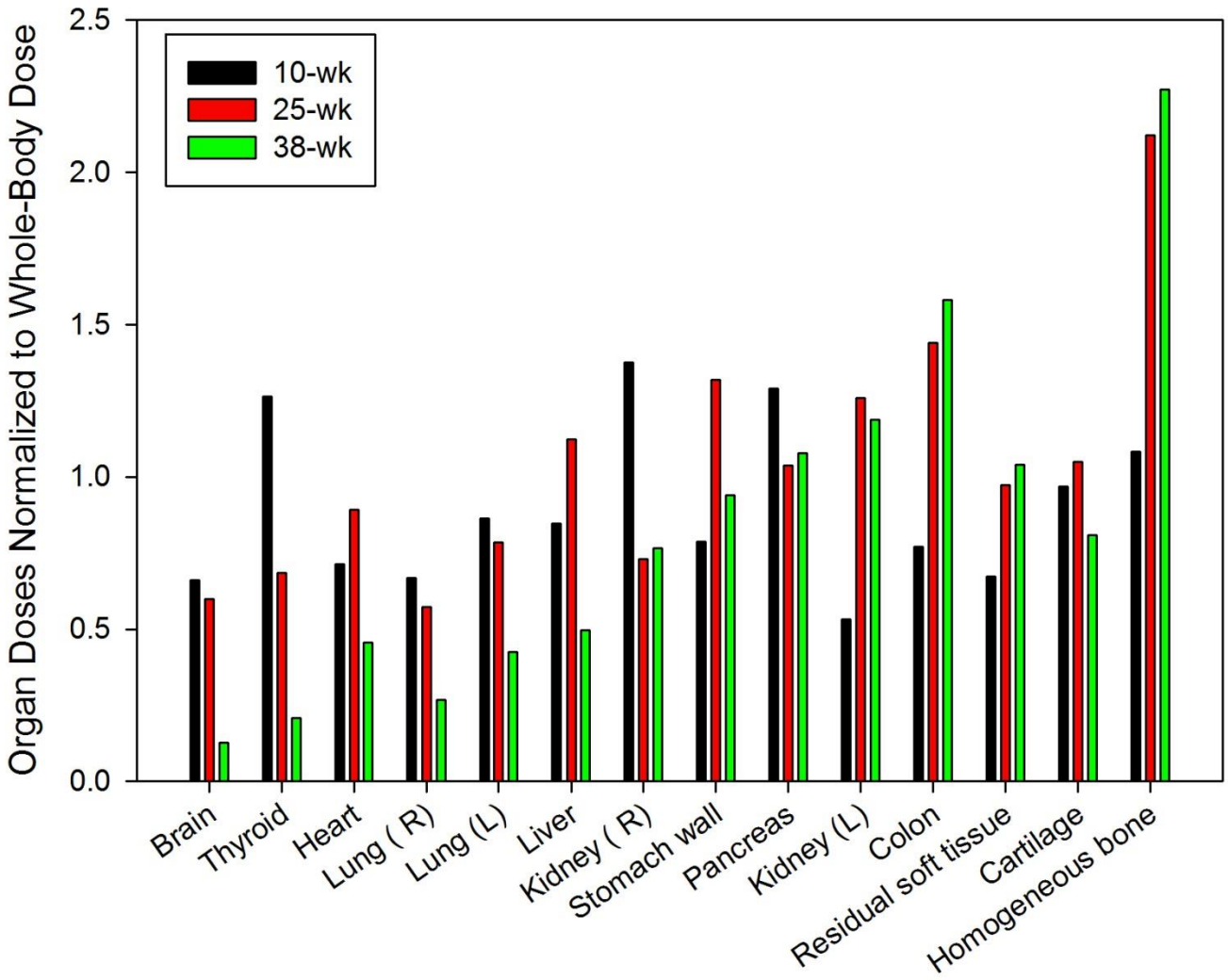

Figure 3-12. Chest exam organ doses normalized to whole-body dose at all three gestational ages

Table 3-1. Percent differences between individual tissues and whole-body doses for abdomen-pelvis exams

	10 weeks Soft-tissue organs	10 weeks Homogeneous bone	25 weeks Soft-tissue organs	25 weeks Homogeneous bone	38 weeks Soft-tissue organs	38 weeks Homogeneous bone
Range	(-26.8% to -0.14%)	(144.2% to 148.0%)	(-13.6% to 15.31 %)	(108.5% to 111.1%)	(13.0% to 21.7 %)	(25.4% to 31.1%)
Average magnitude	12.37%	146.00%	5.60%	109.80%	6.20%	29.00%

CHAPTER 4
CONCLUSIONS AND FUTURE WORK

The goal of this study was to better understand the relative differences in absorbed fetal doses due to CT exams performed on the pregnant female. Comparison between individual fetal organs and the often-reported whole-body dose as functions of fetal and maternal size were discussed. Using the UF reference pregnant female models that contain fetal phantoms with age-dependent organ and bone composition several models with varying sizes of maternal adipose layer were developed at 10, 25, and 38 weeks of gestation. These models allowed for organ-level and bone-level radiation dosimetry.

MCNPX was used to simulated abdomen-pelvis and chest CT exams at 120 kVp, with an assumed tube current-time product of 100 mAs per rotation and a pitch of 0.828. Chest exam fetal doses were at most 1.2 mGy and should not cause significant increases in cancer risks. It was observed that for the abdomen-pelvis exam, soft-tissue organ doses were relatively equivalent to the calculated whole-body dose. However, the skeletal doses were almost as much as 2.5 times larger than the whole-body dose in the 25- and 38-week models. This large difference could result in misleading low childhood leukemia risk estimates if the whole-body dose were to be used instead of the skeletal dose.

This study will be submitted for publication later this year after further improvements are applied to the methodology used. As described in the previous sections, one of the discoveries made was that the fetal size threshold after which differences between whole-body and homogeneous bone doses become relevant lies

somewhere between 10 and 25 weeks of gestation. This issue will be further investigated to find when exactly these differences start to become significant.

Furthermore, it will be worthwhile in the future to explore organ dose differences within a given gestational age as a function of maternal size. This will be done by calculating the doses using retrospectively-collected mAs values from image sets already available.

Although whole-body fetal dose is often the only quantity quoted in CT dosimetry, the imaging community should be aware that although soft-tissue organ doses are very similar to this number, the skeletal dose can be more than twice as large as the whole-body dose. This result could have large implications when using these doses to assess childhood leukemia risks when the models become available.

LIST OF REFERENCES

1. E. Lazarus, C. Debenedectis, D. North, P.K. Spencer, W.W. Mayo-Smith, "Utilization of imaging in pregnant patients: 10-year review of 5270 examinations in 3285 patients--1997-2006," Radiology **251**, 517-524 (2009).

2. C.H. McCollough, B.A. Schueler, T.D. Atwell, N.N. Braun, D.M. Regner, D.L. Brown, A.J. LeRoy, "Radiation exposure and pregnancy: when should we be concerned?" Radiographics **27**, 909-17; discussion 917-8 (2007).

3. M.R. Toglia and J.G. Weg, "Venous thromboembolism during pregnancy," N. Engl. J. Med. **335**, 108-114 (1996).

4. S. Jha, A. Ho, M. Bhargavan, J.B. Owen, J.H. Sunshine, "Imaging evaluation for suspected pulmonary embolism: what do emergency physicians and radiologists say?" AJR Am. J. Roentgenol. **194**, W38-48 (2010).

5. S.K. Doshi, I.S. Negus, J.M. Oduko, "Fetal radiation dose from CT pulmonary angiography in late pregnancy: a phantom study," Br. J. Radiol. **81**, 653-658 (2008).

6. G. Augustin and M. Majerovic, "Non-obstetrical acute abdomen during pregnancy," Eur. J. Obstet. Gynecol. Reprod. Biol. **131**, 4-12 (2007).

7. M.K. Shetty, N.M. Garrett, W.S. Carpenter, Y.P. Shah, C. Roberts, "Abdominal computed tomography during pregnancy for suspected appendicitis: a 5-year experience at a maternity hospital," Semin. Ultrasound CT MR **31**, 8-13 (2010).

8. M.M. Chen, F.V. Coakley, A. Kaimal, R.K. Laros Jr, "Guidelines for computed tomography and magnetic resonance imaging use during pregnancy and lactation," Obstet. Gynecol. **112**, 333-340 (2008).

9. T. Ueberrueck, A. Koch, L. Meyer, M. Hinkel, I. Gastinger, "Ninety-four appendectomies for suspected acute appendicitis during pregnancy," World J. Surg. **28**, 508-511 (2004).

10. A.B. Weingold, "Appendicitis in pregnancy," Clin. Obstet. Gynecol. **26**, 801-809 (1983).

11. S. Maslovitz, G. Gutman, J.B. Lessing, M.J. Kupferminc, R. Gamzu, "The significance of clinical signs and blood indices for the diagnosis of appendicitis during pregnancy," Gynecol. Obstet. Invest. **56**, 188-191 (2003).

12. M.K. Shetty, "Abdominal Computed Tomography During Pregnancy: A Review of Indications and Fetal Radiation Exposure Issues," Seminars in Ultrasound, CT and MRI **31**, 3-7 (2010).

13. M. Remy-Jardin, M. Pistolesi, L.R. Goodman, W.B. Gefter, A. Gottschalk, J.R. Mayo, H.D. Sostman, "Management of suspected acute pulmonary embolism in the era of CT angiography: a statement from the Fleischner Society," Radiology **245**, 315-329 (2007).

14. A. Oto, R.D. Ernst, R. Shah, M. Koroglu, G. Chaljub, A.F. Gei, N. Zacharias, G. Saade, "Right-lower-quadrant pain and suspected appendicitis in pregnant women: evaluation with MR imaging--initial experience," Radiology **234**, 445-451 (2005).

15. E. Lazarus, W.W. Mayo-Smith, M.B. Mainiero, P.K. Spencer, "CT in the evaluation of nontraumatic abdominal pain in pregnant women," Radiology **244**, 784-790 (2007).

16. "International Commission on Radiological Protection," Ann ICRP **84**, 1-43 (2000).

17. M.G. Stabin, E.E. Watson, M. Cristy, J.C. Ryman, K.F. Eckerman, J.L. Davis, D. Marshall, M.K. Gehlen, "Mathematical models and specific absorbed fractions of photon energy in the nonpregnant adult female and at the end of each trimester of pregnancy," Oak Ridge National Laboratory, Oak Ridge, TN, ORNL/TM-12907 (1995).

18. C. Shi and X.G. Xu, "Development of a 30-week-pregnant female tomographic model from computed tomography (CT) images for Monte Carlo organ dose calculations," Med. Phys. **31**, 2491-2497 (2004).

19. E. Angel, C.V. Wellnitz, M.M. Goodsitt, N. Yaghmai, J.J. DeMarco, C.H. Cagnon, J.W. Sayre, D.D. Cody, D.M. Stevens, A.N. Primak, C.H. McCollough, M. McNitt-Gray, "Radiation dose to the fetus for pregnant patients undergoing multidetector CT imaging: Monte Carlo simulations estimating fetal dose for a range of gestational age and patient size," Radiology **249**, 220-7 (2008).

20. J. Chen, "Mathematical models of the embryo and fetus for use in radiological protection," Health Phys. **86**, 285-295 (2004).

21. X.G. Xu, V. Taranenko, J. Zhang, C. Shi, "A boundary-representation method for designing whole-body radiation dosimetry models: pregnant females at the ends of three gestational periods--RPI-P3, -P6 and -P9," Phys. Med. Biol. **52**, 7023-7044 (2007).

22. M.R. Maynard, J.W. Geyer, J.P. Aris, R.Y. Shifrin, W. Bolch, "The UF family of hybrid phantoms of the developing human fetus for computational radiation dosimetry," Phys. Med. Biol. **56**, 4839-79 (2011).

23. C. Lee, D. Lodwick, J. Hurtado, D. Pafundi, J.L. Williams, W.E. Bolch, "The UF family of reference hybrid phantoms for computational radiation dosimetry," Phys. Med. Biol. **55**, 339-363 (2010).

24. D. Pafundi, C. Lee, C. Watchman, V. Bourke, J. Aris, N. Shagina, J. Harrison, T. Fell, W. Bolch, "An image-based skeletal tissue model for the ICRP reference newborn," Phys. Med. Biol. **54**, 4497-4531 (2009).

25. J. Gu, B. Bednarz, P.F. Caracappa, X.G. Xu, "The development, validation and application of a multi-detector CT (MDCT) scanner model for assessing organ doses to the pregnant patient and the fetus using Monte Carlo simulations," Phys. Med. Biol. **54**, 2699-2717 (2009).

BIOGRAPHICAL SKETCH

Nelia Sánchez Long was born Nelia Sánchez Monreal in Havana, Cuba. She attended high school in Miami, and graduated cum laude with a Bachelor of Science in nuclear engineering from the University of Florida in May 2010. She graduated with a Master of Science in biomedical engineering with a concentration in medical physics from the University of Florida in May 2013, and is currently pursuing a doctorate degree in the same field.